J. Fluid Mech. (2025), *vol.* 1018, A5, doi:10.1017/jfm.2025.10529

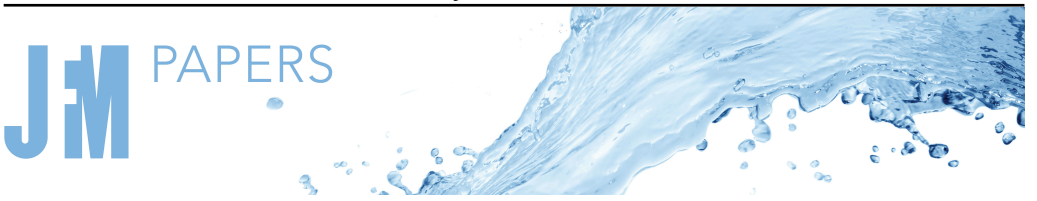

Determination of the characteristic length of electrosprays operating in the cone-jet mode

Marco Magnani[1], **Manuel Gamero-Castaño**[1] **and Juan Fernández de la Mora**[2]

[1]Department of Mechanical and Aerospace Engineering, University of California, Irvine, CA 92697, USA

[2]Yale University, New Haven, CT 06511, USA

Corresponding author: Manuel Gamero-Castaño, mgameroc@uci.edu

(Received 13 March 2025; revised 8 June 2025; accepted 22 July 2025)

Gamero-Castaño and colleagues have reported that a large number of calculated shapes for electrified cone jets collapse into a nearly universal geometry when scaled with a characteristic length R_G previously introduced by Gañán-Calvo *et al.* (*J. Aerosol Sci.*, vol. 25, 1994, pp. 1121–1142). The theoretical reasons for that unexpected success were, however, unclear. Recently, Pérez-Lorenzo & Fernández de la Mora (*J. Fluid Mech.*, vol. 931, 2022, A4) have noted that a slightly different length scale L_j is suggested by the asymptotic jet structure inferred by Gañán-Calvo (*Phys. Rev. Lett.*, vol. 79, 1997, pp. 217–220) from energy conservation and the hypothesis that the asymptotic electric field is that given by Taylor's static model. This article aims to identify which of these two scales best collapses calculated cone-jet structures, and whether there is an alternative superior one. The characteristic lengths are tested against a large set of numerical solutions of a cone-jet model. The effectiveness of each scaling is determined through analyses based on the standard deviation of the numerical solutions. Despite the slight difference between R_G and L_j, this analysis clearly identifies L_j as the most accurate scaling for all cone-jet parameters tested. Differentiating between both scales would not have been possible with experimental measurements, but requires the use of high-fidelity numerical solutions. Surprisingly, the success of L_j is not limited to the jet region, but extends to the cone and the neck. These findings provide a slightly superior scaling enjoying a considerably firmer theoretical basis.

Key words: aerosols/atomization, electrohydrodynamic effects, capillary flows

1. Introduction

There have been numerous attempts at determining the various length scales governing electrified liquid cone jets. Initial efforts were directed at the characteristic radius in the neck region, where the Taylor cone begins to evolve into a jet. A first hypothesis defining an inertial radius R_i was that the capillary pressure $\sim\gamma/R_i$ would become comparable with the dynamic pressure $\sim\rho Q^2/{R_i}^4$, resulting in

$$R_i \propto \left(\frac{\rho Q^2}{\gamma}\right)^{1/3}, \tag{1.1}$$

where Q is the flow rate of liquid, ρ its density and γ the surface tension at the liquid–gas interface (Turnbull 1989; Fernández de la Mora *et al.* 1990). The approximate agreement initially obtained with a few observations was nevertheless incomplete in view of the known strong dependence of the jet radius on the electrical conductivity K of the liquid. Fernández de la Mora & Loscertales (1994) studied systematically this dependence. This was done primarily through measurements not of the jet radius, but of the emitted current I, which they showed was well approximated by

$$I = f(\varepsilon)\,(\gamma K Q)^{1/2}, \tag{1.2}$$

where $f(\varepsilon)$ is a function of the dielectric constant ε of the liquid. Their attempt to rationalise this strikingly simple scaling led them to a model where the increasing electrical resistance of the cone and the increasing liquid velocity as the neck region was approached would eventually disrupt Taylor's hypothesis of an equipotential meniscus (Taylor 1964). This approach also defined the following characteristic electrical relaxation radius R_r:

$$R_r = \left(\frac{\varepsilon_0 Q}{K}\right)^{1/3}, \tag{1.3}$$

with a dependence on ε that is ignored for present purposes; ε_0 is the vacuum permittivity. Fernández de la Mora & Loscertales (1994) reasoned that the jet radius would scale with R_r, and included a few experimental observations suggesting that this was not unreasonable. This point was more systematically supported by various later sets of measurements of the size of the drops produced by the breakup of the jet (Rosell-Llompart & Fernández de la Mora 1994; Chen & Pui 1997; Gañán-Calvo *et al.* 1997). The ratio between these two early length scales introduced a dimensionless flow rate quantity (Gañán-Calvo *et al.* 1993; Fernández de la Mora & Loscertales 1994),

$$\Pi_Q = \frac{\rho K Q}{\gamma \varepsilon_0} = \left(\frac{R_i}{R_r}\right)^3, \tag{1.4}$$

which has been widely used subsequently. Quantity Π_Q will play a role in the present discussion because most of the various other characteristic lengths that have been proposed can be written as the product of a flow-rate-independent length, $l_o = ({\varepsilon_0}^2\gamma/\rho K^2)^{1/3}$, times Π_Q raised to a certain power a.

Gañán-Calvo and collaborators, postulating that the surface charge is in electrostatic equilibrium everywhere in the cone jet, deduced the following expression for the current (Gañán-Calvo *et al.* 1993):

$$I \cong 2.47(\gamma K Q)^{1/2}, \tag{1.5}$$

introduced a third characteristic length for the radius of the jet (Gañán-Calvo *et al.* 1994):

$$R_G = \left(\frac{\varepsilon_0 \rho Q^3}{K\gamma}\right)^{1/6}, \tag{1.6}$$

and a different characteristic length for the axial extent of the transition region:

$$Z_G = \left(\frac{\rho^2 K Q^3}{\varepsilon_0 \gamma^2}\right)^{1/3}, \tag{1.7}$$

based on several simplified balances (Gañán-Calvo 2004; Gañán-Calvo *et al.* 2018). It is important to note that the argument leading to the radial scale (1.6) requires the existence of the axial scale (1.7), because it postulates an approximation for the current determined by Taylor's potential (Taylor 1964), $I \sim K R^2 E_t \sim K R^2 [\gamma/(\varepsilon_0 L)]^{1/2}$, and the characteristic radius R and axial length L must have the R_G and Z_G scalings, respectively, in order for the current to follow (1.5).

It initially seemed difficult to establish which of these characteristic lengths would best fit existing experiments. The power a is often a small number, while the dimensionless flow rate at which stable cone jets can be formed spans a limited range. The difficulty was further compounded by the fact that some of the measured lengths relate to different parts of the jet, and by the difficulty in measuring submicrometric features with the accuracy needed to resolve the small differences in the length scales: the neck region is perhaps better characterised by R_r, while the radius of the jet in the breakup region is possibly better represented by the measured droplet radius (which furthermore exhibits a distribution that must be reconciled with the radius of the jet). Since the radius of the jet is many times smaller than its length, and is continually shrinking as it is accelerated by the electric field, it is conceivable that different length scales will best describe the various pieces of the cone jet. This issue will nevertheless be later seen to be less serious than it might initially appear because the asymptotic jet shape involves a rather slow variation with the axial position x, as $R \propto x^{-1/8}$ (Gañán-Calvo 1997).

A breakthrough in the effort to identify the optimal characteristic length for the cone jet was enabled by a series of studies by Gamero-Castaño and colleagues. First, Gamero-Castaño & Hruby (2001) invented a vacuum method allowing the measurement of the jet radius at its breakup point. This study showed that the scale R_G fitted well all measured drop radii, and fitted them much better than the scale R_r. In a later extension, focused on the dissipation of energy in cone jets (Gamero-Castaño 2010), it was shown that both the radial and axial lengths scale well with a single characteristic length, R_G. In fact, when the positions of the surface of cone jets obtained numerically were scaled with R_G, all profiles approximately collapsed into a single universal shape over a wide range of flow rates, electrical conductivities, dielectric constants and viscosities (Gamero-Castaño & Magnani 2019). Most relevant in this latter study was the fact that these many cone jets did approximately collapse into a single shape, not just at the neck or at a certain downstream point, but through the whole cone, the jet and the transition region. The new numerical evidence was accordingly far stronger than that previously available from drop diameter measurements. The debate about the correct characteristic length hence appeared to be clearly settled experimentally and computationally in favour of R_G.

Nevertheless, the theoretical basis for the successful R_G scale is not wholly persuasive for several reasons. In the first place, it is now apparent that the same radial and axial length scales apply in the transition and jet regions, while the justifications provided by

Gañán-Calvo and collaborators (Gañán-Calvo 2004; Gañán-Calvo *et al.* 2018) required different scales for the jet radius (1.6) and length (1.7). Second, the energy balance used by Gañán-Calvo *et al.* (2018) to obtain the R_G scale may be simplified (the work done by the electric field is balanced against the increase in kinetic energy of the liquid), because it neglects dissipation which is more significant than the increase in kinetic energy in a long section of the transition region (see Gamero-Castaño & Magnani 2019). Third, the $R \propto Q^{1/2}$ dependence found by Gamero-Castaño (2010), and therefore the support for R_G, was based on the remarkable Q-independence of experimental retarding potential curves of electrosprayed droplets. However, these retarding potential curves have a finite spread, which introduces uncertainty in the derivation from the curve of a single voltage value connected to the physics of the jet. This uncertainty would invalidate the strict Q-independence of the retarding potential curve and make it difficult to distinguish between length scales with very similar Q dependencies, i.e. similar values of the exponent a.

1.1. *Asymptotic jet structure and its length scale L_j*

We have noted that the variation of the radius of the jet between its neck and breakup region is not unduly large. This important point may be ascertained because of the following considerations first put together by Gañán-Calvo (1997) to obtain an analytic description of the jet shape far downstream. The neck region is associated with a certain dissipation where electrical energy is turned into heat due to the finite conductivity of the medium. This dissipative region, however, ends soon, once the conductive current through the bulk of the liquid dies out and the dominant charge-carrying mechanism, convection of the surface charge, is non-dissipative. Thereafter, the following energy conservation equation applies approximately:

$$\frac{\rho Q^3}{2\pi^2 R^4} + I\Phi = \text{constant}, \tag{1.8}$$

where mass conservation relates the fluid velocity u to the flow rate via $Q = \pi R^2 u$. Gañán-Calvo then assumes that, to first-order approximation, the potential along the jet surface is given by Taylor's potential (Taylor 1964):

$$\Phi(x) = -\phi_T \left(\frac{\gamma x}{\varepsilon_0}\right)^{1/2}, \tag{1.9}$$

where ϕ_T is a constant of order unity, given by Taylor's theory of the electrohydrostatic cone. In this picture the origin of the potential is at $x = 0$, where the kinetic energy is also zero, which nullifies the constant in (1.8). Combining (1.8) and (1.9), one finds

$$R^4 x^{1/2} = \frac{\rho Q^3}{2\pi^2 I \phi_T} \left(\frac{\varepsilon_0}{\gamma}\right)^{1/2}. \tag{1.10}$$

One consequence of (1.10) already noted is that the radius decreases rather slowly, as $R \propto x^{-1/8}$, such that even a very long jet changes modestly its radius. Two additional implications of (1.10) were first noted by Pérez-Lorenzo & Fernández de la Mora (2022). The first is that (1.10) implies a characteristic jet length L_j:

$$L_j^{9/2} = \frac{\rho Q^3}{2\pi^2 I \phi_T} \left(\frac{\varepsilon_0}{\gamma}\right)^{1/2}, \tag{1.11}$$

in terms of which the asymptotic jet shape is universal. In choosing this scale we have assumed that the axial and radial length scales coincide. This is not necessarily true in the

jet region. However, if one seeks (perhaps unjustifiably) a characteristic length that will collapse both the jet and the cone, there is no room for two scales because the cone angle is fixed in Taylor's electrostatic model. The second consequence of (1.10) noted by Pérez-Lorenzo & Fernández de la Mora (2022) is that the jet length scale defined in (1.11) is hardly distinguishable from R_G. For concreteness, and using (1.2) to express the current,

$$\frac{L_j}{R_G} \approxeq \frac{\Pi_Q{}^{1/18}}{(2\pi\phi_T)^{2/9}}. \tag{1.12}$$

The small power of Π_Q relating these two length scales would appear to make it rather difficult to distinguish between them.

The goal of this article is to determine the appropriateness of several length scales for collapsing the surfaces of cone jets, namely L_j, R_G and R_r used in both the radial and axial directions, and the combined $R_G{-}Z_G$. The surfaces are numerical solutions of a first-principles model computed over a broad range of operational conditions. We find that both R_G and L_j are close to the optimum length scale, and that the latter performs better. Irrespective of the slightly different fitting merits of these two almost identical scales, the simple rationalisation of the new length scale L_j obtained from (1.8)–(1.10) provides now a readily understandable theoretical explanation for why both do such a good job in collapsing the calculated electrified meniscus shapes, at least in the far-downstream region.

2. Cone-jet model and analysis methodology

The cone jet is modelled using the leaky-dielectric formulation (Melcher & Taylor 1969; Saville 1997). A detailed description can be found in Gamero-Castaño & Magnani (2019) and Magnani & Gamero-Castaño (2024). The model is axisymmetric and steady state, and restricted to isothermal conditions in the present study. It solves for the velocity and pressure fields in the liquid, the position of the free surface $R(x)$, the surface charge and the electric potential inside the cone jet and surrounding vacuum. An important feature of the model is the use of Taylor's potential as far-field boundary condition, which yields a solution that is independent of the geometry of the emitter and ground electrodes. Experimentally, this corresponds to a cone jet in which the length and diameter of the jet are orders of magnitude smaller than any geometric dimension such as the diameter of the emitter or the distance between the emitter and ground electrode. The origin of coordinates for the Taylor potential (1.9) also fixes the origin of coordinates of the cone-jet model; because of this, the numerical solution is not invariant to an axial translation. The solution is a parametric function of three dimensionless numbers, namely the dimensionless flow rate Π_Q, the dielectric constant ε and the electrohydrodynamic Reynolds number

$$Re = \left(\frac{\varepsilon_0\rho\gamma^2}{K\mu^3}\right)^{1/3}, \tag{2.1}$$

Reynolds number henceforth. Terms Π_Q, Re and ε are the only dimensionless numbers appearing in the isothermal model equations, and therefore the position of the surface is given by

$$\tilde{R} = f\left(\tilde{x};\, \Pi_Q,\, Re,\, \varepsilon\right), \tag{2.2}$$

where we use a tilde to signify a dimensionless variable (dimensional variables are uncapped throughout the article). There are different criteria for defining a characteristic length scale. Here, we adopt the expectation that there exist radial and axial scale functions

of the dimensionless flow rate, Reynolds number and dielectric constant, $L_r(\Pi_Q, Re, \varepsilon)$ and $L_x(\Pi_Q, Re, \varepsilon)$, such that

$$\frac{R}{L_r} = f\left(\frac{x}{L_x}\right). \tag{2.3}$$

The reduction of (2.2) into (2.3) is not generally possible, but the findings of Gamero-Castaño (2010) and Gamero-Castaño & Magnani (2019) indicate that this collapsing of the surfaces into a single function is approximately valid in cone jets. For simplicity we restrict $L_r(\Pi_Q, Re, \varepsilon)$ and $L_x(\Pi_Q, Re, \varepsilon)$ to power laws. The analysis is simplified by defining a general characteristic length, $L_\mathcal{C}$, from which the different scales proposed in the literature can be obtained as special cases. Length $L_\mathcal{C}$ is a combination of powers of the various relevant liquid properties and the flow rate:

$$L_\mathcal{C} = Q^a \mu^{-b} \varepsilon^c \rho^d \gamma^e K^f {\varepsilon_0}^g, \tag{2.4}$$

where μ stands for the viscosity. Length $L_\mathcal{C}$ can be recast as the product of the flow-rate-independent length l_o times powers of the dimensionless flow rate, the Reynolds number and the dielectric constant:

$$L_\mathcal{C} = \left(\frac{{\varepsilon_0}^2\gamma}{\rho K^2}\right)^{1/3} \left(\frac{\rho K Q}{\varepsilon_0 \gamma}\right)^a \left(\frac{\varepsilon_0 \rho \gamma^2}{K\mu^3}\right)^{b/3} \varepsilon^c = l_o {\Pi_Q}^a Re^b \varepsilon^c. \tag{2.5}$$

The characteristic lengths discussed in § 1 omit dependencies on the Reynolds number and the dielectric constant, $b = 0$ and $c = 0$, and are defined by the following values of a:

(i) $a = 1/3 \rightarrow R_r$,
(ii) $a = 1/2 \rightarrow R_G$,
(iii) $a = 5/9 \rightarrow L_j$,
(iv) $a = 1 \rightarrow Z_G$.

Alternative length scales can be studied by varying the values of a, b and c.

We evaluate the appropriateness of a length scale by quantifying how effectively it collapses all $R(x)$ solutions into a single function. We use a normalised standard deviation to measure this:

$$s_n(y) = \frac{1}{\overline{y}} \sqrt{\frac{1}{N} \sum_{i=1}^{N} |y_i - \overline{y}|^2}, \tag{2.6}$$

where y is the variable being studied, N the number of samples and $\overline{y}$ the mean value of the variable. Furthermore, the performance of a length scale over an axial interval $[x_a, x_b]$ is quantified by averaging the standard deviation:

$$\overline{s_n}(y) = \frac{1}{x_b - x_a} \int_{x_a}^{x_b} s_n(y(x)) \mathrm{d}x. \tag{2.7}$$

The simulations include the following ionic liquids: 1-ethyl-3-methylimidazolium bis((trifluoromethyl)sulphonyl)imide, 1-butyl-3-methylimidazolium tricyanomethane, 1-ethyl-3-methylimidazolium trifluoroacetate, ethylammonium nitrate, 1-decyl-3-methylimidazolium bis(trifluoromethylsulphonyl)amide and 2-hydroxyethylammonium lactate (see table 1). The physical properties of the ionic liquids are obtained from the Ionic Liquid Database (Kazakov *et al.* 2022). We have calculated 146 solutions covering wide ranges of the dimensionless flow rate, $10 \leqslant \Pi_Q \leqslant 5500$, the Reynolds number, $0.0033 \leqslant Re \leqslant 0.747$, and the dielectric constant, $12.7 \leqslant \varepsilon \leqslant 85.6$. All solutions are

Name	CAS no.	Solutions	Π_Q	Re	ε
1-Butyl-3-methylimidazolium tricyanomethanide	878027-73-7	22	10–1000	0.0093	12.7
1-Decyl-3-methylimidazolium bis(trifluoromethylsulphonyl)amide	433337-23-6	3	100–1000	0.0033	14.9
1-Ethyl-3-methylimidazolium bis(trifluoromethylsulphonyl)amide	174899-82-2	47	10–4000	0.0075–0.747	13.1
1-Ethyl-3-methylimidazolium trifluoroacetate	174899-65-1	28	10–5000	0.0085	14.6
2-Hydroxyethylammonium lactate	68815-69-0	17	50–4000	0.0053	85.6
Ethylammonium nitrate	22113-86-6	29	10–5500	0.0061	27.1

Table 1. Numerical solutions used in the analysis: liquids considered, number of solutions for each liquid and ranges of Π_Q, Re and ε investigated.

isothermal, calculated at 21 °C. For a description of thermal effects in cone jets we refer the reader to Gamero-Castaño (2019) and Magnani & Gamero-Castaño (2024).

3. Analysis of the characteristic lengths

Figure 1 shows the current as a function of the dimensionless flow rate for all cone jets simulated. The current is made dimensionless with the scale $I_o = \sqrt{\varepsilon_0 \gamma^2/\rho}$, to facilitate comparison with the traditional scaling law $I/I_o \propto {\Pi_Q}^{1/2}$, equation (1.2) (Gañán-Calvo *et al.* 1993; Fernández de la Mora & Loscertales 1994). At flow rates $\Pi_Q \lesssim 250$, the data are well fitted by $I/I_o = 2.45{\Pi_Q}^{1/2} + 0.895$, in excellent agreement with expression (1.5) found analytically by Gañán-Calvo *et al.* (1993) and with the best fit reported by Gañán-Calvo *et al.* (2018), $I/I_o = 2.5{\Pi_Q}^{1/2}$, for experimental data including 54 different electrolytes. The data with higher flow rates are also well approximated by a square-root law with a slightly lower coefficient. The values for the cone jets with the highest dielectric constant ($\varepsilon = 85.6$) and with highest Reynolds number ($Re = 0.747$) suggest that the current increases with Re and decreases with ε, although these dependencies are weak compared with the dependence on Π_Q. Two more features are worth mentioning. First, although the larger dimensionless flow rates may seem high, they are typical in cone jets of ionic liquids. For example, Gamero-Castaño & Cisquella-Serra (2021) report measurements of EMI-Im cone jets in the range $612 \leqslant \Pi_Q \leqslant 3630$; furthermore, Caballero-Pérez & Gamero-Castaño (2025) have demonstrated EMI-Im flow rates as low as $\Pi_Q \sim 10$. Second, these numerical solutions provide a more accurate tool for probing the physics than experiments, not only because many features of cone jets are not accessible by the latter, but also because of the fidelity of the numerical solution. For example, figure 1 shows that, under isothermal operation, I/I_o is nearly a single-valued function of Π_Q that follows well a power law (a square root with a negligible constant term). This result is rarely reproduced with this precision in experimental data. For example, figure 7 in Gañán-Calvo *et al.* (2018) summarising experimental data for 54 different electrolytes shows that although the data generally fall near $I/I_o = 2.5{\Pi_Q}^{1/2}$, the measurements for a given liquid are better fitted by power laws with exponents slightly different from 1/2, with coefficients different from 2.5 and potentially having a constant

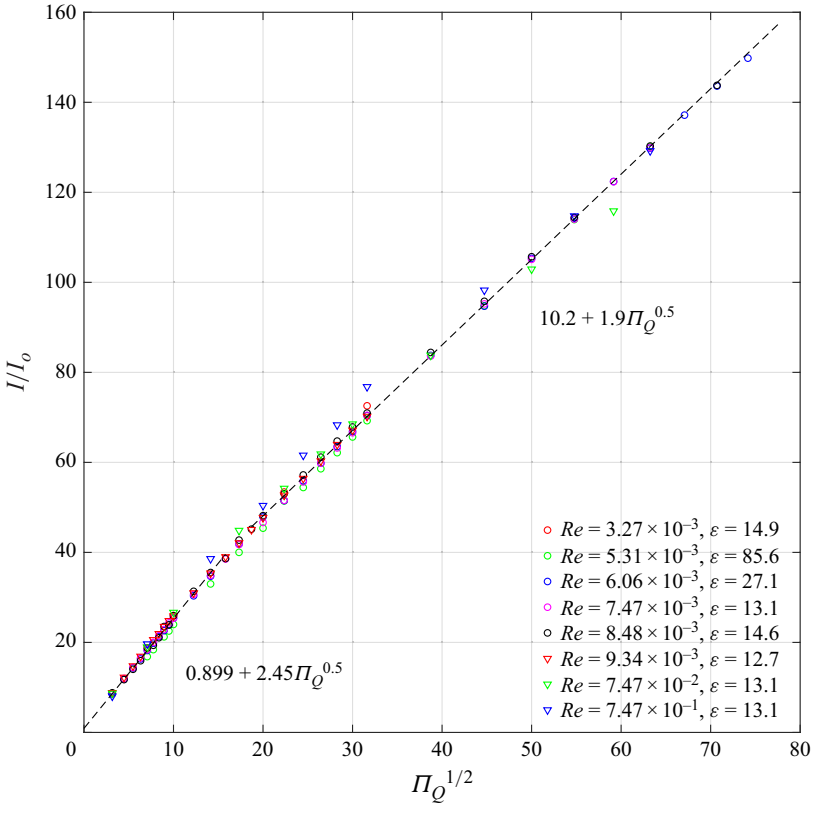

Figure 1. Total current emitted by the electrospray, plotted as a function of Π_Q.

term. This is to be expected since there are a number of issues that make it difficult to obtain experimental data with the fidelity achievable in a numerical simulation.

Figure 2 illustrates the definition of the characteristic length as the scale needed to collapse disparate cone-jet surfaces into a narrow band. Throughout the article and unless otherwise noted, the origin of the axial coordinate in the figures is the origin of the axial coordinate in the numerical solution or, equivalently, the origin of coordinates for the Taylor potential. Figure 2(*a*,*b*) shows the position of the surface for most cone jets simulated. Because of the wide ranges of dimensionless flow rates, dielectric constants and Reynolds numbers investigated, the radii span several orders of magnitude. For example, the radius at which the bulk conduction and surface current coincide, that is, the radius of the current crossover, varies between 2.87 nm and 2.42 μm across the simulations. However, when normalising the radial and axial coordinates with appropriate length scales, for example L_j in figure 2(*c*), the various profiles collapse within a narrow band. The appropriateness of L_j is surprising because while the solution is a function of three dimensionless numbers, only one, Π_Q, is included in L_j; furthermore, there is no indication in the model that both coordinates must have the same scale. These two features are likely preventing a full collapse of the profiles into a single function. Figure 2(*d*) shows that the combined $R_G - Z_G$ scales do not collapse the cone-jet profiles as well as the single L_j scale.

Figure 3(*a*) shows the normalised standard deviation of the radius of the cone jet, (2.6), as a function of the axial coordinate for four scalings: R_r, R_G and L_j employed in both the radial and axial directions, and the combined $R_G - Z_G$ scales. We have normalised the axial coordinate with the average position where the surface current I_s is 90 % of the total

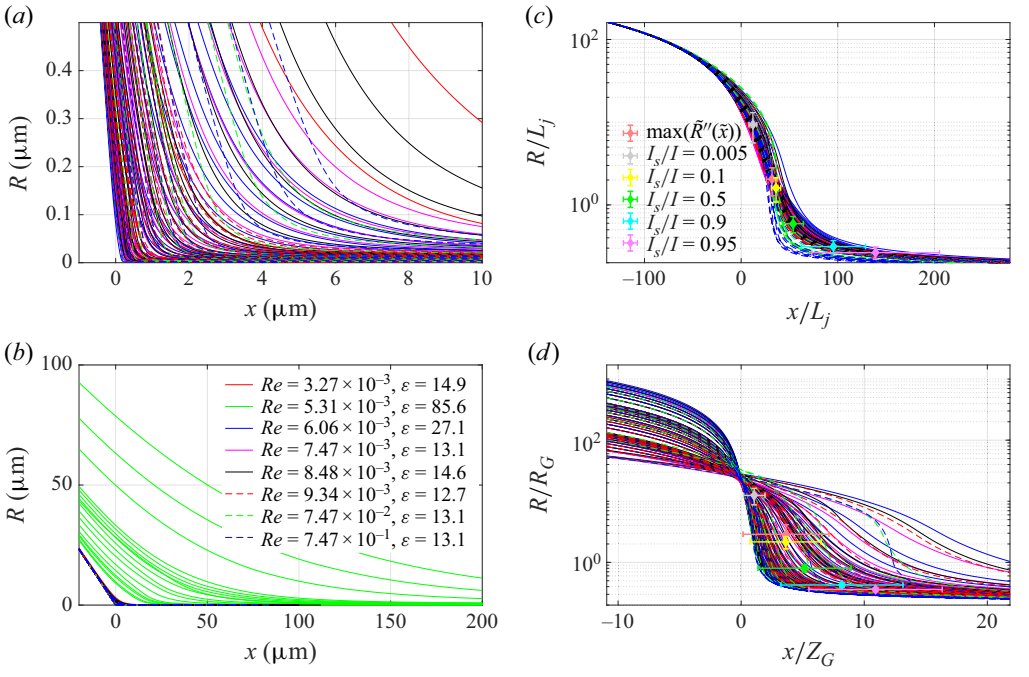

Figure 2. (*a*,*b*) Dimensional cone-jet profiles; (*c*) cone-jet profiles scaled with L_j; (*d*) cone-jet profiles scaled with R_G and Z_G. The scaled profiles include the radius and axial positions (and their standard deviations) for several values of the surface current I_s and the maximum of $\tilde{R}''(\tilde{x})$.

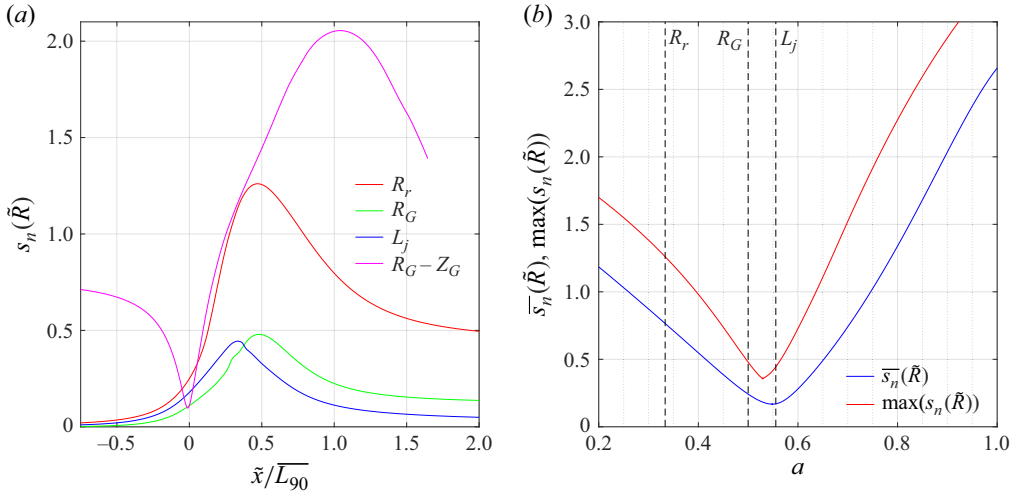

Figure 3. (*a*) Normalised standard deviation of the radius of the cone jet, $\tilde{R}(\tilde{x})$, for four different length scale combinations: $a_r = a_x = 1/3$; $a_r = a_x = 1/2$; $a_r = a_x = 5/9$; and $a_r = 1/2$, $a_x = 1$. (*b*) Average standard deviation of the cone-jet radius in $0 \leqslant \tilde{x} \leqslant 2\overline{L_{90}}$, and maximum value of the normalised standard deviation, as a function of the length-scale power a.

current, $\overline{L_{90}}$. This is important for a direct comparison between the scales, as increasing the value of the power a in (2.5) compresses the curves horizontally. Using R_G and L_j in both directions collapse the profiles well, although L_j is superior almost everywhere in the jet, especially far downstream where conduction current is negligible. The R_G-Z_G combination collapses the profiles significantly worse everywhere along the cone jet. The reduction of the cone-jet profiles by the L_j scale is significant: the maximum disagreement is 0.444 at $\tilde{x}/\overline{L_{90}} = 0.327$, for a range of radii spanning over three orders of magnitude, between 11.1 nm and 14.3 μm, at this axial position. Figure 3(*b*) measures the quality of the scale $l_o \Pi_Q{}^a$ when used for both the radial and axial coordinates, as a function of the power a. We do this by averaging the normalised standard deviation of the radius in the interval $0 \leqslant \tilde{x} \leqslant 2\overline{L_{90}}$. We also plot the maximum value of the normalised standard deviation of the radius within this interval. Value $a = 0.548$ minimises the average standard deviation, while $a = 0.529$ minimises the maximum standard deviation. Both optimums are close to the value $a = 5/9$ for the L_j scale, with the minimum of the average standard deviation being closest. These two minima provide the optimal values for a in the transition region (where the maximum of $S_n(\tilde{R})$ is located) and all along the jet (which dictates the value of $\overline{s_n}(\tilde{R})$). Value $a = 5/9$ for the L_j scale is very close to both optimum values.

The Taylor potential is a boundary condition for the model, and therefore the numerical solution is not invariant to an axial translation. Because of this and how the characteristic length is defined, (2.3), an axial translation should not be used in an attempt to improve the collapse of the profiles. Furthermore, a translation preferentially reduces the average standard deviation of profiles normalised with a poor scale, and therefore reduces the sensitivity of the analysis for determining the optimum scaling. This is illustrated in figures 4 and 5. Figures 4 plots the normalised standard deviation of the profiles, scaled with R_G and L_j in both directions and the combined R_G-Z_G scales, for three translation cases: zero translation (solid lines); when the position of the maximum of $\tilde{R}''(\tilde{x})$ is subtracted from the axial coordinate of each profile (dashed lines, $\tilde{x}_{R''}$ label); and when subtracting the position of the current crossover point (dash-dotted lines, $\tilde{x}_{50}$ label). For a better comparison in the plot, after computing each normalised standard deviation curve we add the average value of the translation to the axial coordinate to realign the curves. While the standard deviation of the profiles normalised with the R_G and L_j scales is barely affected by the $\tilde{x}_{R''}$ translation and modestly changes with the $\tilde{x}_{50}$ translation, the standard deviation of the profiles normalised with the combined R_G-Z_G scales improves greatly with either translation (although the collapsing of the profiles still remains worse than when employing the R_G or L_j scales in both directions). Figure 5 shows cone-jet profiles with filled circles indicating the position of the maximum of $\tilde{R}''(\tilde{x})$. When the profiles are normalised with the L_j scale in both directions, an axial translation aligning the profiles to the intrinsic position of the maximum of $\tilde{R}''(\tilde{x})$ does not improve the collapse of the profiles because they are already close to each other without the need of a translation. On the other hand, the large separation between the profiles when they are scaled with R_G-Z_G greatly improves when the translation enforces the alignment of the positions of the $\tilde{R}''(\tilde{x})$ maxima, i.e. when the translation enforces the profiles to be similar around this intrinsic point. This apparent improvement is helped by the very slow and monotonic decrease of the radius with the axial position, which makes the normalised standard deviation of the profiles small in the far-downstream region, regardless of a translation. Note also that instead of using a translation that aligns the profiles at an intrinsic point (for example the position of the maximum of $\tilde{R}''(\tilde{x})$ or the position of a given value of the I_s/I ratio), a more arbitrary translation could have been used, for example one specific to each profile in such a way that the average standard deviation for a given scaling is

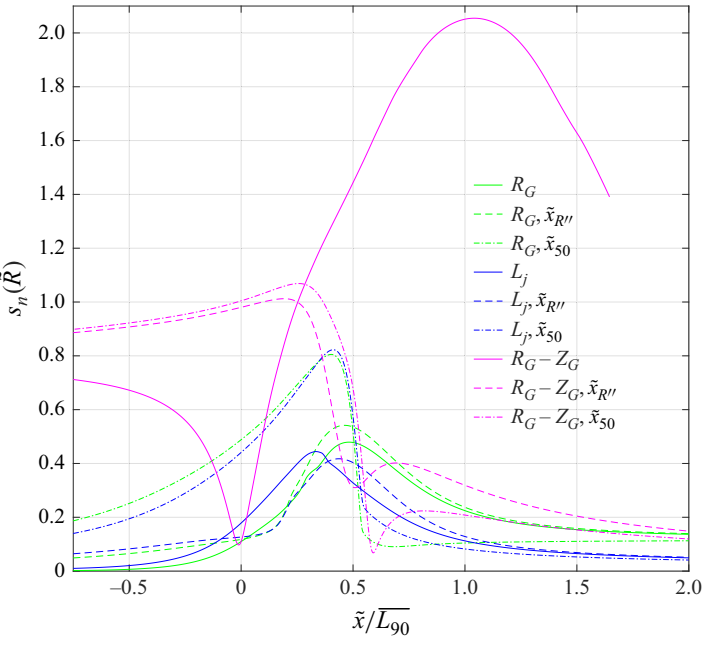

Figure 4. Normalised standard deviation of the cone-jet profiles for several scalings and axial translations. Here $\tilde{x}_{R''}$ designates translation by the axial position of the maximum of $\tilde{R}''(\tilde{x})$, while $\tilde{x}_{50}$ corresponds to a translation by the position of the current crossover point.

minimised. This translation choice would make it even more difficult to determine the optimum scaling, since almost any scaling could be used to produce an apparent good collapse of the profiles. A corollary of this observation is that it will be difficult to do this scaling analysis with images of experimental cone jets, because the analysis will likely rely on an *ad hoc* criterion for fixing the origin of coordinates of each profile.

Figure 6 shows the average standard deviation of the cone-jet radius, computed in the interval $0 \leqslant \tilde{x} \leqslant 2\overline{L_{90}}$, as a function of the powers a_r and a_x of the length scale in the radial and axial directions, respectively. We continue neglecting a dependence of the length scales on the Reynolds number and the dielectric constant. Value $a_r = 0.568$ combined with $a_x = 0.529$, marked in the plot by a red circle, produces the optimum scaling with an average standard deviation $\overline{s_n}(\tilde{R}) = 0.163$. Among the reported length scales L_j, with $a_r = a_x = 5/9$ and $\overline{s_n}(\tilde{R}) = 0.168$, is closest to the optimum. This scaling is significantly better than the combined $R_G - Z_G$ for the radial and axial directions, which has an average standard deviation $\overline{s_n}(\tilde{R}) = 1.44$. The scaling R_G used in both directions is also close to the optimum, $\overline{s_n}(\tilde{R}) = 0.240$, while $\overline{s_n}(\tilde{R}) = 0.762$ for R_r, $a_r = a_x = 1/3$. An important feature of this plot is that the optimum value nearly fulfils the constraint

$$a_r = -\frac{1}{8}a_x + \frac{5}{8} \tag{3.1}$$

imposed by (1.10). This further supports the reasoning leading to the L_j length scale.

Figure 7 shows the average standard deviation for scalings that depend on the dimensionless flow rate and the Reynolds number, and on the dimensionless flow rate and the dielectric constant. In both cases the same characteristic length is used in both the radial and axial directions. The optimum scaling decreases with the Reynolds number,

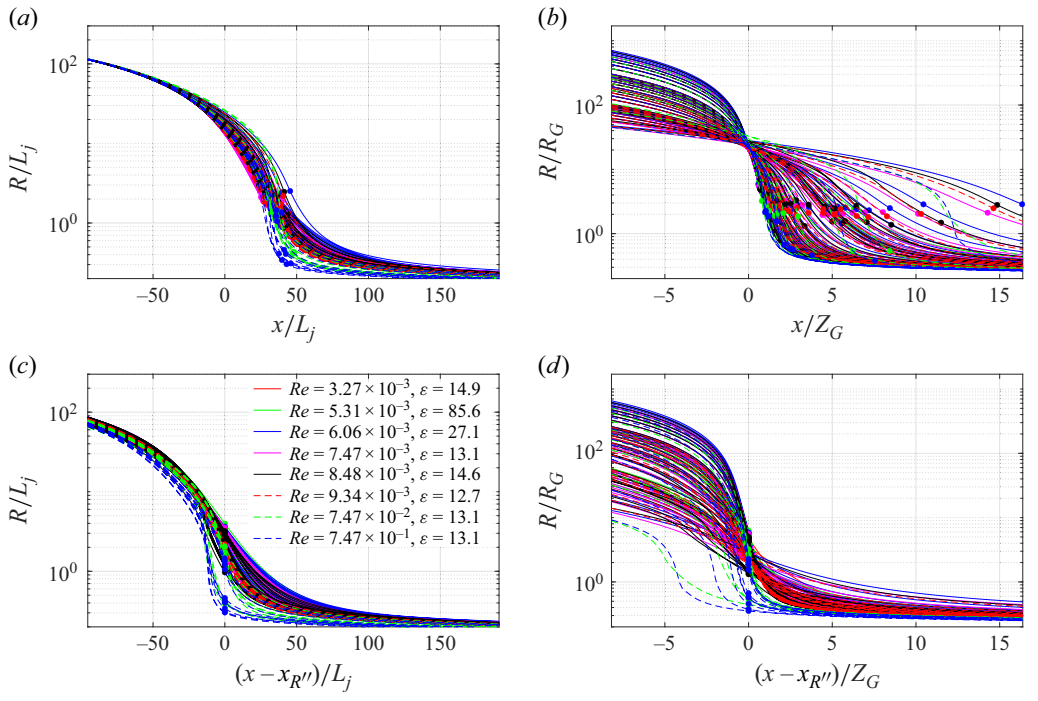

Figure 5. Cone-jet profiles with the position of the maximum of $\tilde{R}''(\tilde{x})$ marked by a filled circle: (*a*) profiles scaled with L_j in both directions; (*b*) profiles scaled with the combined $R_G - Z_G$ scales; (*c*) profiles with axial translation $x_{R''}$ scaled with L_j; (*d*) profiles with axial translation $x_{R''}$ scaled with $R_G - Z_G$.

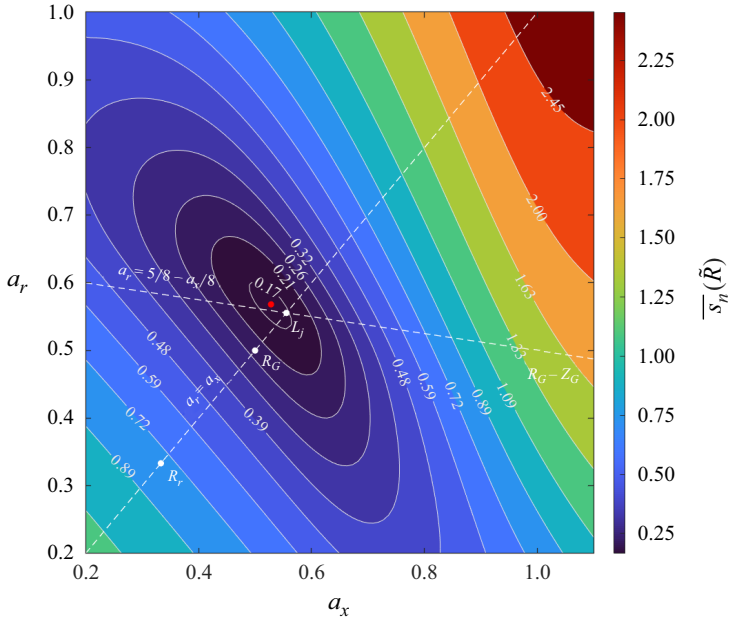

Figure 6. Average standard deviation of the cone-jet radius in $0 \leqslant \tilde{x} \leqslant 2\overline{L_{90}}$, as a function of the length-scale powers in the radial and axial directions.

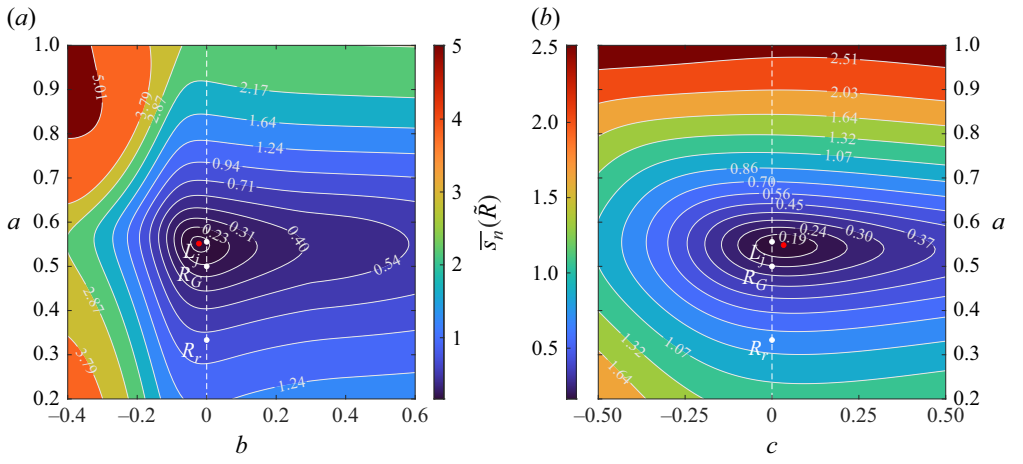

Figure 7. Average standard deviation of the cone-jet radius in $0 \leqslant \tilde{x} \leqslant 2\overline{L_{90}}$, as a function of the powers in the scaling (*a*) $L_r = L_x = l_o \Pi_Q{}^a Re^b$, combined effects of the dimensionless flow rate and Reynolds number; and (*b*) $L_r = L_x = l_o \Pi_Q{}^a \varepsilon^c$, combined effects of the dimensionless flow rate and dielectric constant.

$a = 0.552$ and $b = -0.022$, and increases with the dielectric constant, $a = 0.548$ and $c = 0.033$, but these dependencies are weak. In both cases L_j nearly coincides with the optimum dependency on the dimensionless flow rate.

Due to the monotonic decrease of the cone-jet radius along the axial coordinate, defining a characteristic length in a manner different from (2.3), such as using the radius at a particular point, is problematic. One possibility is to specify the characteristic radius at a particular value of the ratio between the surface current and the total current, I_s/I, since this variable is an intrinsic coordinate for the cone jet ranging from 0 to 1 as x goes from $-\infty$ to ∞. Figure 8 illustrates the problem with this approach. We plot the radii, normalised with l_o, at $I_s/I = 0.05$, 0.15, 0.50, 0.85 and 0.95 as a function of the dimensionless flow rate. The data are well fitted by power laws, except for a few radii associated with the largest Reynolds number and lowest flow rates hinting at a weaker dependency on Re. However, the exponents of the fittings vary significantly, between 0.393 for $I_s/I = 0.05$ and 0.487 for $I_s/I = 0.95$. The radial length scale resulting from this definition is not unique, and it would be arbitrary to choose a particular I_s/I value.

Figures 1 and 7(*b*) suggest a weak dependence of the current and the characteristic length on the dielectric constant, although more detailed analysis (e.g. computing states at constant dimensionless flow rate and Reynolds number while varying the dielectric constant) would be needed to quantify it. Gañán-Calvo and collaborators (Gañán-Calvo *et al.* 1993, 1994; Gañán-Calvo 2004; Gañán-Calvo *et al.* 2018) have proposed that the surface charge σ is in electrostatic quasi-equilibrium, $\sigma \cong \varepsilon_0 E_n^o$ or equivalently $\varepsilon E_n^i / E_n^o \ll 1$, everywhere along the cone jet, which would indeed make the solution quasi-independent of the dielectric constant (E_n^o and E_n^i are the normal components of the electric field in the outer and inner sides of the surface, respectively). However, the surface charge in our solutions can be substantially smaller than its equilibrium value, and therefore a weak dependence on the dielectric constant is likely. This can be seen in the profiles of the ratio $\sigma/(\varepsilon_0 E_n^o)$ in figure 9(*a*) for several numerical solutions. Although the surface charge is in quasi-equilibrium sufficiently upstream and downstream from the origin, its value is significantly smaller than $\varepsilon_0 E_n^o$ near the current crossover point, $x = x_{50}$,

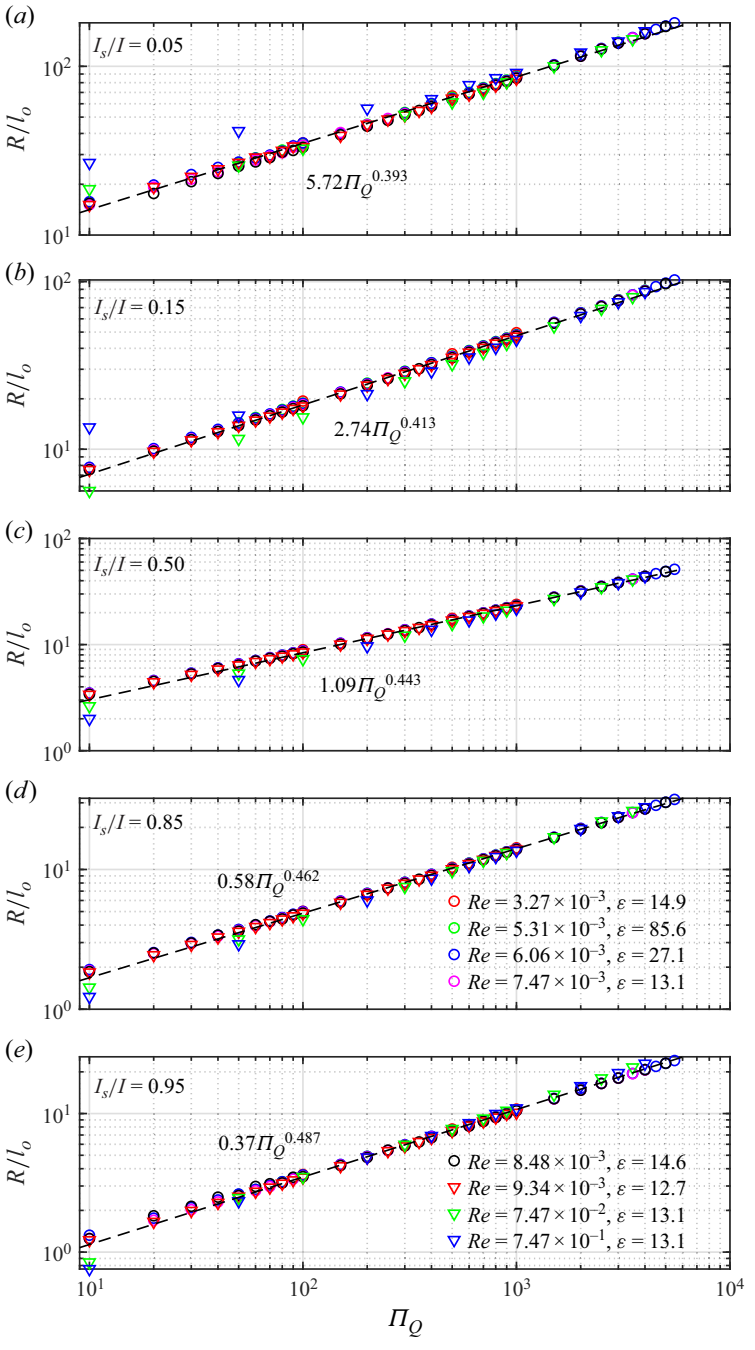

Figure 8. Radius of the cone jet at different values of the ratio between the surface and total currents, $I_s/I =$ 0.05, 0.15, 0.5, 0.85 and 0.95, plotted as a function of the dimensionless flow rate.

the divergence increasing at decreasing dimensionless flow rate. Figure 9(*b*) shows the minimum value of the ratio $\sigma/(\varepsilon_0 E_n^o)$ for all cases considered in this study. It is worth noting that the maximum separation from equilibrium increases with both $\varepsilon/(\pi\Pi_Q{}^{1/2})$ and the Reynolds number. Gamero-Castaño & Magnani (2019) identify $\varepsilon/(\pi\Pi_Q{}^{1/2})$

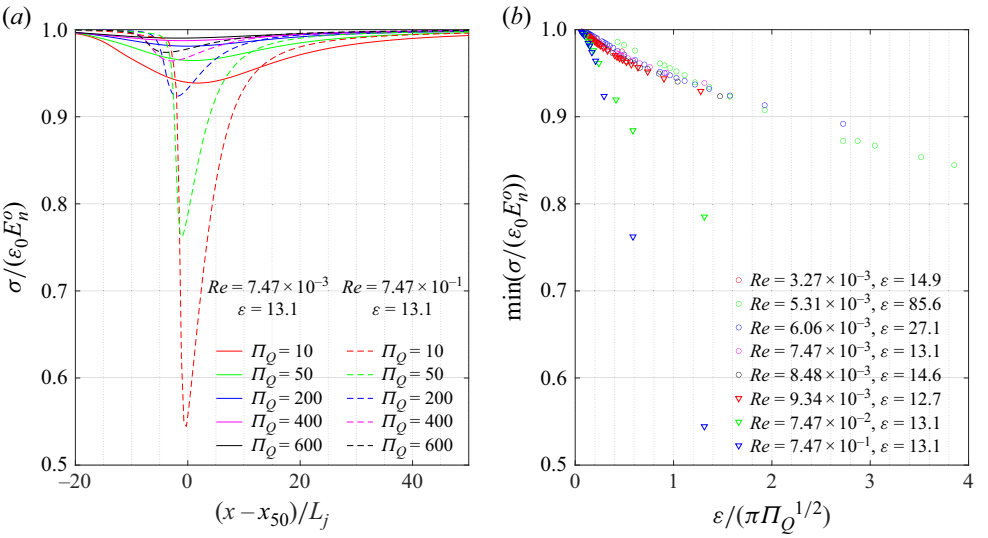

Figure 9. (*a*) Ratio between the surface charge and its equilibrium value for the several cone jets; (*b*) maximum value of the ratio $\sigma/(\varepsilon_0 E_n^o)$ for all simulations.

with the ratio between the electric relaxation time and the flow residence time, $t_e/t_f \simeq \varepsilon/(\pi \Pi_Q{}^{1/2})$. Gañán-Calvo and collaborators propose that $t_e/t_f \ll 1$ is always fulfilled in cone jets, since this guarantees zero volumetric charge density in the bulk and leads to a surface charge in equilibrium. Although $t_e/t_f \ll 1$ is a sufficient condition for the volumetric charge density to be zero, it is not a required condition. In fact, Melcher & Taylor (1969) show that if the electric conduction is adequately represented by Ohm's law with a constant electrical conductivity and the fluid particle lines do not traverse upstream regions containing a net volumetric charge density (two conditions that are fulfilled in typical cone jets), the volumetric charge density is zero everywhere regardless of whether $t_e/t_f \ll 1$ is fulfilled.

4. Conclusions

We have investigated the appropriateness of various length scales for collapsing the surfaces of cone jets. The surfaces are numerical solutions of a first-principles model based on the leaky-dielectric assumption, computed in a broad range of operational conditions (Magnani & Gamero-Castaño 2024). The scales $L_j = l_o \Pi_Q{}^{5/9}$ (Pérez-Lorenzo & Fernández de la Mora 2022) and $R_G = l_o \Pi_Q{}^{1/2}$ (Gañán-Calvo *et al.* 2018) applied to both the radial and axial coordinates collapse the surfaces well; however, L_j is closest to the optimum scaling $L_r = l_o \Pi_Q{}^{0.568}$ and $L_x = l_o \Pi_Q{}^{0.529}$ found by statistical analysis. This is significant, because the appropriateness of L_j now provides a theoretical basis for the length scale, namely the constraint $L_r{}^4 L_x{}^{1/2} \propto \Pi_Q{}^{5/2}$ between the radial and axial scales imposed by conservation of mechanical energy in the fully developed jet (Pérez-Lorenzo & Fernández de la Mora 2022). The optimum scaling nearly fulfils this constraint. Differentiating between these similar scales would not have been possible with experimental measurements, highlighting the usefulness of high-fidelity numerical calculations in the investigation of electrosprays. Although the geometry of the cone jet is

also a function of the Reynolds number and the dielectric constant (Gamero-Castaño & Magnani 2019), these dependencies are weak and can be ignored in the expression for the characteristic scale. We have examined the possibility of defining the radial scale as the jet radius defined by a particular ratio between the surface and total currents I_s/I. However, this radial scale depends on the value of I_s/I, and adopting a particular scale is therefore arbitrary.

Funding. This work was funded by the Air Force Office of Scientific Research, awards no. FA9550-21-1-0200 at UCI and no. FA9550-22-1-0097 at Yale.

Declaration of interests. The authors report no conflict of interest.

References

Caballero-Pérez, M. & Gamero-Castaño, M. 2025 High specific impulse electrospray propulsion with small capillary emitters. arXiv:2504.00474.

Chen, D.R. & Pui, D.Y.H. 1997 Experimental investigation of scaling laws for electrospraying: dielectric constant effect. *Aerosol Sci. Technol.* **27** (3), 367–380.

Fernández de la Mora, J. & Loscertales, I.G. 1994 The current emitted by highly conducting Taylor cones. *J. Fluid Mech.* **260**, 155–184.

Fernández de la Mora, J., Navascues, J., Fernández, F. & Rosell-Llompart, J. 1990 Generation of submicron monodisperse aerosols in electrosprays. *J. Aerosol Sci.* **21**, S673–S676.

Gamero-Castaño, M. 2010 Energy dissipation in electrosprays and the geometric scaling of the transition region of cone–jets. *J. Fluid Mech.* **662**, 493–513.

Gamero-Castaño, M. 2019 Dissipation in cone-jet electrosprays and departure from isothermal operation. *Phys. Rev. E* **99**, 061101.

Gamero-Castaño, M. & Cisquella-Serra, A. 2021 Electrosprays of highly conducting liquids: a study of droplet and ion emission based on retarding potential and time-of-flight spectrometry. *Phys. Rev. Fluids* **6** (1), 013701.

Gamero-Castaño, M. & Hruby, V. 2001 Electrospray as a source of nanoparticles for efficient colloid thrusters. *J. Propul. Power* **17** (5), 977–987.

Gamero-Castaño, M. & Magnani, M. 2019 Numerical simulation of electrospraying in the cone-jet mode. *J. Fluid Mech.* **859**, 247–267.

Gañán-Calvo, A.M. 1997 Cone-jet analytical extension of Taylor's electrostatic solution and the asymptotic universal scaling laws in electrospraying. *Phys. Rev. Lett.* **79** (2), 217–220.

Gañán-Calvo, A.M. 2004 On the general scaling theory for electrospraying. *J. Fluid Mech.* **507**, 203–212a.

Gañán-Calvo, A.M., Barrero, A. & Pantano-Rubiño, C. 1993 The electrohydrodynamics of electrified conical menisci. *J. Aerosol Sci.* **24**, S19–S20.

Gañán-Calvo, A.M., Davila, J. & Barrero, A. 1997 Current and droplet size in the electrospraying of liquids. Scaling laws. *J. Aerosol Sci.* **28** (2), 249–275.

Gañán-Calvo, A.M., Lasheras, J.C., Dávila, J. & Barrero, A. 1994 The electrostatic spray emitted from an electrified conical meniscus. *J. Aerosol Sci.* **25** (6), 1121–1142.

Gañán-Calvo, A.M., López-Herrera, J.M., Herrada, M.A., Ramos, A. & Montanero, J.M. 2018 Review on the physics of electrospray: From electrokinetics to the operating conditions of single and coaxial Taylor cone-jets, and AC electrospray. *J. Aerosol Sci.* **125**, 32–56.

Kazakov, A., Magee, J.W., Chirico, R.D., Paulechka, E., Diky, V., Muzny, C.D., Kroenlein, K. & Frenkel, M. 2022 Nist standard reference database 147: Nist ionic liquids database-(ilthermo) version 2.0. http://ilthermo.boulder.nist.gov

Magnani, M. & Gamero-Castaño, M. 2024 Analysis of self-heating in electrosprays operating in the cone-jet mode. *J. Fluid Mech.* **980**, A40.

Melcher, J.R. & Taylor, G.I. 1969 Electrohydrodynamics: a review of the role of interfacial shear stresses. *Annu. Rev. Fluid Mech.* **1** (1), 111–146.

Pérez-Lorenzo, L.J. & Fernández de la Mora, J. 2022 Probing electrically driven nanojets by energy and mass analysis in vacuo. *J. Fluid Mech.* **931**, A4.

Rosell-Llompart, J. & Fernández de la Mora, J. 1994 Generation of monodisperse droplets 0.3 to 4 μm in diameter from electrified cone-jets of highly conducting and viscous liquids. *J. Aerosol Sci.* **25** (6), 1093–1119.

SAVILLE, D.A. 1997 Electrohydrodynamics: the Taylor–Melcher leaky dielectric model. *Annu. Rev. Fluid Mech.* **29** (1), 27–64.

TAYLOR, G.I. 1964 Disintegration of water drops in an electric field. *Proc. R. Soc. Lond. A. Math. Phys. Sci.* **280** (1382), 383–397.

TURNBULL, R.J. 1989 Self-acceleration of a charged jet. *IEEE Trans. Indust. Appl.* **25** (4), 699–704.